Electrochimica Acta, Vol. 26, pp. 261–273.
Pergamon Press Ltd. 1981. Printed in Great Britain.

0013–4686/81/0201–0261 $02.00/0

POTENTIODYNAMIC BEHAVIOUR OF THE RHODIUM/H_2SO_4(aq) INTERFACE IN THE POTENTIAL RANGE OF THE HYDROGEN AND OXYGEN ELECTROSORPTION

C. PALLOTTA, N. R. DE TACCONI and A. J. ARVIA

Division Electroquimica, Instituto de Investigaciones Fisicoquimicas Teoricas y Applicadas (INIFTA). Sucursal 4, Casilla de Correo 16, 1900 La Plata, Argentina

Abstract—The electrochemical response of Rh/H_2SO_4(aq) interfaces at 25°C, subjected to different potential–time perturbation programs in the potential range of H and O electrosorption and H and O electrodesorption is reported. The H electrosorption and H electrodesorption involve the participation of at least two distinguishable adsorption states. The degree of reversibility of the corresponding electrochemical processes is appreciably influenced by the history of the electrode including the type of perturbation applied to the electrode in the O electrosorption potential range.

The O electrosorption and O electrodesorption involve the formation of different surface species as it is deduced either from the charge balance or from the kinetic response of the electrochemical interface. The early stages of the anodic reaction are interpreted through a reversible charge transfer comprising the formation of OH adsorbed species which later undergoes electrochemical and chemical reactions yielding different O-containing species. The existence of the various O-containing surface species as well as the influence of the most stable ones in the H electrosorption potential range is evidenced through their potentiodynamic electrodesorption. The kinetic results of the O electrosorption are discussed in terms of aging mechanisms including anion adsorption.

INTRODUCTION

The electrochemical sorption processes of H and O on noble metals is particularly relevant when attempting to understand the structure of the electrochemical interface in relation to the stability of metals in contact with electrolyte solutions and to the processes involved in the activation of noble metal electrodes. Most of these studies were devoted to Pt and Au electrodes in aqueous electrolytes subjected to a large variety of electrochemical perturbation conditions[1–25]. The general features of the electroformation and the electroreduction of H and O monolayers on those metals were interpreted through composite reaction patterns which involve electrochemical as well as chemical stages combined either in series or in parallel[19, 20, 22]. The recently developed kinetic models deal with the influence of both the type of electrosorptive bond between the first metal atom layer and the electrosorbed species, and the specific adsorption of ions and molecules at the electrochemical interface. The electrosorptive bond energy depends both on the crystallographic structure of the metal and on the electrolyte composition. The influence of specifically adsorbed species is determined by a compromise between the kinetics of the adsorption processes, its time constant and the potential range of the electrical perturbation applied to the electrochemical interface. This implies, therefore, that the electrochemical sorption processes should involve the competition among solvent molecules, adsorbable ions and electrosorbable species for each particular type of adsorption site. Likewise, the possible surface restructuring associated with the aging of the electrosorbed species when the electrosorptive bond energy is relatively high also contributes to the complexity of those reactions. Consequently, through the response of the electrochemical interface to properly adjusted sets of potentiodynamic perturbations certain aspects of the complex electrochemical reaction can be emphasized.

Within the potential range of the thermodynamic stability of water the Rh/H_2SO_4(aq) interface behaves to some extent rather similarly to the Pt/H_2SO_4(aq) interface. The literature[1–25] reveals that the knowledge of the sorption processes related to the H and O species on Rh is fairly limited. In the potential range where the O electrosorption and electrodesorption takes place the comparable results obtained with simple triangular potential sweeps are reasonably coincident although they furnish no definite evidence of any anodic or cathodic current peak multiplicity which could be related to some type of aging[27, 29]. On the other hand, in the potential range of the H adatoms the available results show that the degree of reversibility of the conjugated electrochemical system is appreciably sensitive to the electrode history.

The present paper deals with the potentiodynamic behaviour of Rh/H_2SO_4 (aq) interfaces. Aging processes related to the O-sorption which are to some extent similar to those already described for the Pt/H_2SO_4 (aq) interface are observed. The aging processes interfere with the electrochemical response of the system throughout the potential range of the thermodynamic stability of water. The formation of tightly bound O-containing electrosorbed species on Rh may account for its electrochemical behaviour in the hydrogen adatom potential range.

EXPERIMENTAL

The experimental arrangement is the same as that already described in previous publications[26, 27]. It consists of a Pyrex glass cell with a system of three

electrodes, namely, a Rh working electrode, either a Pt or Rh counterelectrode, and a hydrogen reference electrode (*hre*) in the solution concentration which was connected through a Luggin capillary.

Polycrystalline spectroscopically pure Rh wire electrodes (Johnson, Matthey and Co., 0.1 cm dia., 0.580 cm^2 apparent area) were used. After prolonged use as anode in H_2SO_4 (aq) electrolytes, subjected to repetitive triangular potential sweeps (RTPS) in the 0 V to 1.5 V range (*hre*), a Rh electrode is greatly activated towards the H adatom electrochemical reactions (Type-I). Otherwise, fresh Rh electrodes and Rh electrodes subjected to high positive potentials in the O_2 evolution potential region were also employed (Type-II).

Type-II electrodes behave more sluggish than Type-I electrodes, particularly with respect to the H-adatoms electrochemical reactions. However, although the two types of electrodes were distinguished, the electrode activation mechanism is not firmly established but independently of it the possibility that vestiges of Pt causes the electrode activation has been experimentally discarded.

The H_2SO_4 solutions (0.1 M and 12 M) were prepared from 98 percent H_2SO_4 (Merck, A. R.) and triply distilled water. Water was obtained through a series of slow distillations from basic permanganate and sulphuric acid containing solutions. The deaerated electrolytes satisfied the purity criterion established through the repetitive voltammetric *E–I* response of the Pt/H_2SO_4 (aq) electrochemical interface in the H-adatoms potential range[28].

The 12 M H_2SO_4 electrolyte was preferred because of the better resolution of the different potentiodynamic current peaks as compared to the more diluted electrolytes[18]. At this concentration the double layer region is more extended than at lower concentrations since the O-electrosorption initiates at more positive potentials. This is probably associated to the increasing surface blocking by the specific adsorption of anions as in the case of the Pt/H_2SO_4 interface[18, 29].

The electrochemical interface was perturbed with different either simple or complex potential perturbation programs. In order to obtain reproducible and comparable responses it was previously subjected to a RTPS between 0 V and 1.5 V, at high potential sweep rates (v) for several cycles. Immediately afterwards, the voltammetric run at the preset perturbation conditions was performed. The potentiodynamic *E–I* displays were initiated either from the cathodic switching potential ($E_{s,c}$) or from the anodic switching potential ($E_{s,a}$) depending on the purpose of the experiment. In the following text the stabilized RTPS *E–I* displays are used as reference. The different potential–time programs applied to the electrochemical interfaces are shown in each figure together with the corresponding potentiodynamic *E–I* displays. The experiments were made at 25°C in N_2 saturated electrolytes.

RESULTS

Preliminary considerations

The stabilized RTPS *E–I* profile run with a Type-I electrode in either 0.1 M or 12 M H_2SO_4 solution at 0.3 V/s within the potential range of the water thermodynamic stability (Fig. 1), exhibits the clear separation of two well known main electrochemical reactions.

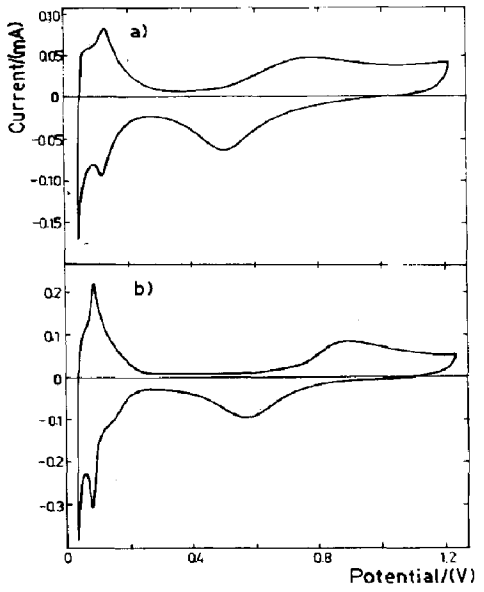

Fig. 1. Potentiodynamic stabilized RTPS *E–I* displays (reference profiles) run at 0.3 V/s and 25°C. Type I-electrode. (a) 0.1 M H_2SO_4; (b) 12 M H_2SO_4.

During the positive going potential scan (PPS), at potentials more negative than 0.2 V the H-electrodesorption takes place, whereas, at potentials more positive than 0.6 V the O-electrosorption occurs. The surface coverage related to the latter covers from a submonolayer up to a few monolayers depending on $E_{s,a}$. The negative going potential scan (NPS) comprises the O-electrodesorption in the 0.9 V to 0.2 V range and the H-electrosorption at potentials more negative than 0.2 V. The NPS profile, contrarily to the PPS, shows a potential range where both the O-electrodesorption and the H-electrosorption occur simultaneously.

The H-electrosorption and H-electrodesorption are characterized by at least two conjugate redox couples. The main one corresponds to the redox system located at *ca* 0.1 V and the second one is related to the anodic and cathodic shoulders located at the positive potential sides of the respective current peaks. The corresponding conjugate redox systems at least at low v exhibit the characteristics of reversible electrochemical reactions. The current peak multiplicity related to the H-adatoms becomes less clear as the electrolyte concentration decreases and simultaneously the overall reaction seems to behave as a process of increasing irreversibility. The same effect is also noticed for the O-electrosorption and O-electrodesorption. The increasing electrolyte concentration apparently produces changes in the energy distribution of the adsorbed species related to both the H- and the O-electrosorption processes. This effect is comparable to the H_2SO_4 concentration influence on the same processes occurring at the Pt/H_2SO_4 (aq) interfaces[29]. Inde-

pendently the broad current peaks related to the O-electrosorption and O-electrodesorption, which apparently exhibit the characteristics of irreversible electrochemical reactions are actually composite *E–I* contours, as described further on. Comparable runs made with Type-II electrodes (Fig. 2) reveal that in these electrodes the separation of the H-adatom current peak potentials as well as the corresponding current peak height distribution are slightly different.

The H- and O-electrosorption charges were preferably evaluated from the PPS because of the appreciable separation of the potential range associated to each of these reactions. Thus, in the 12 M H_2SO_4 this separation comes up to *ca* 0.4 V. On the other hand, the overall anodic and cathodic charges are strongly dependent on $E_{s,a}$ and v. Likewise, the charge in the H-adatom potential range is perturbed by the possible contribution of H_2 unless $E_{s,c}$ is slightly more positive than 0 V. However, for the aim of the present work the charge balance associated to the O-electrosorption and O-electrodesorption is the most relevant as analysed further on.

The influence of $E_{s,a}$ *and* $E_{s,c}$ *on the potentiodynamic* E–I *profile*

The RTPS *E–I* profiles (0.01 V/s $\leqslant v \leqslant$ 0.2 V/s) initiated from $E_{s,c} = 0.02$ V up to a stepwise either increasing or decreasing $E_{s,a}$ (Fig. 2) permit one to understand the genesis and characteristics of the composite current peak structure related to the O-electrosorption and the O-electrodesorption as well as the influence of the latter on those taking place in the potential range of the H-adatom electrode reaction. Thus, when $E_{s,a}$ decreases the O-electrodesorption current peak is appreciably modified in size and shape until it approaches a limiting current when $E_{s,a}$ is more negative than 0.8 V. Simultaneously the H-adatom redox couple located at more positive potentials becomes less distinguishable.

Complementary runs were also made by keeping $E_{s,a}$ constant and changing $E_{s,c}$ stepwise from 1.20 V to 0.10 V (Fig. 3a). Furthermore, after changing $E_{s,c}$ ten RTPS were run before recording the corresponding *E–I* display (Fig. 3b). As $E_{s,c}$ gradually becomes more negative the charges playing part in both the cathodic and the anodic processes increase and simultaneously, a new cathodic current peak tends to form at potentials more negative than those of the main cathodic current peak observed in the reference *E–I* display. In both types of experiments once $E_{s,c}$ exceeds the potential of the O-electrodesorption current peak, a progressive current increase at a constant potential is observed for both the anodic and the cathodic processes. Then, a further shift of $E_{s,c}$ downwards produces an *E–I* display approaching the shape of the reference *E–I* profile. All these changes are more noticeable when the perturbation program includes a RTPS preceding the *E–I* record (Fig. 3b). Under these circumstances the potential perturbation program approaches the one used for the potentiodynamic aging of O-containing films on noble metal electrodes[30, 31].

The overall modifications of the O electroreduction *E–I* profile depends upon both $E_{s,a}$ and $E_{s,c}$. The largest modification corresponds to an $E_{s,c}$ value where the removal of about 60 per cent of the charge of the O electrodesorption current peak ($Q_{o,c}$) in the reference *E/I* profile is involved.

The anodic and the cathodic charges in the 0.7 V *to* 1.6 V *range*

The *E–I* displays run between $E_{s,c} = 0.02$ V and 0.50 V $\leqslant E_{s,a} \leqslant$ 1.6 V (Fig. 2) show that the anodic charge (Q_a) depends on v. At any $E_{s,a}$ value, the Q_a *vs* v plot exhibits an initial decay and a constant $(Q_a)_L$ charge when $v \geqslant 0.2$ V/s (Fig. 4). Both $(Q_a)_L$ and $(Q_a)^\circ$, the charge extrapolated at $v \to 0$, increases with $E_{s,a}$ (Figs. 4 and 5). As a matter of fact the $(Q_a)^\circ$ *vs* $E_{s,a}$ plot (Fig. 5) coincides with the results obtained for the Rh/H_2SO_4(aq) interface by applying potentiostatic pulses[16]. The $(Q_a)^\circ$ *vs* $E_{s,a}$ plot shows two linear portions, namely one from 0 to 1.15 V and another from 1.25 V up to 1.6 V.

On the other hand, the Q_a *vs* $E_{s,a}$ plots obtained

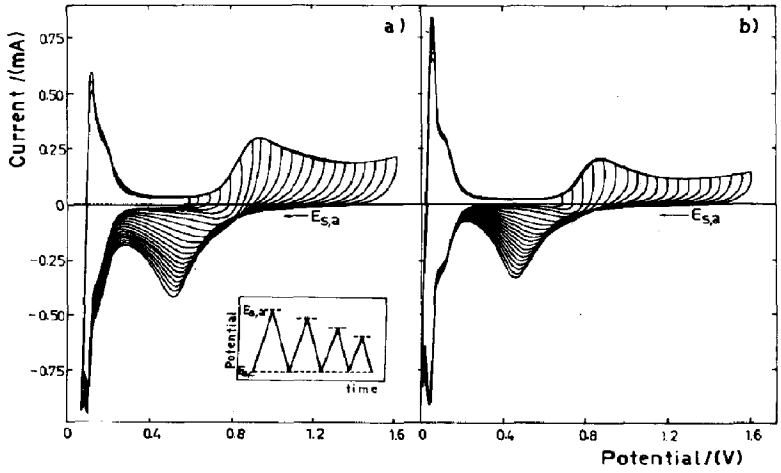

Fig. 2. Potentiodynamic *E–I* displays run under single triangular potential sweep (STPS) at 0.3 V/s (a) (Type I electrode) and at 0.25 V/s (b) (Type II electrode) in 12 M H_2SO_4 covering a constant $E_{s,c}$ and gradually decreasing $E_{s,a}$. The potential–time program is indicated in the figure.

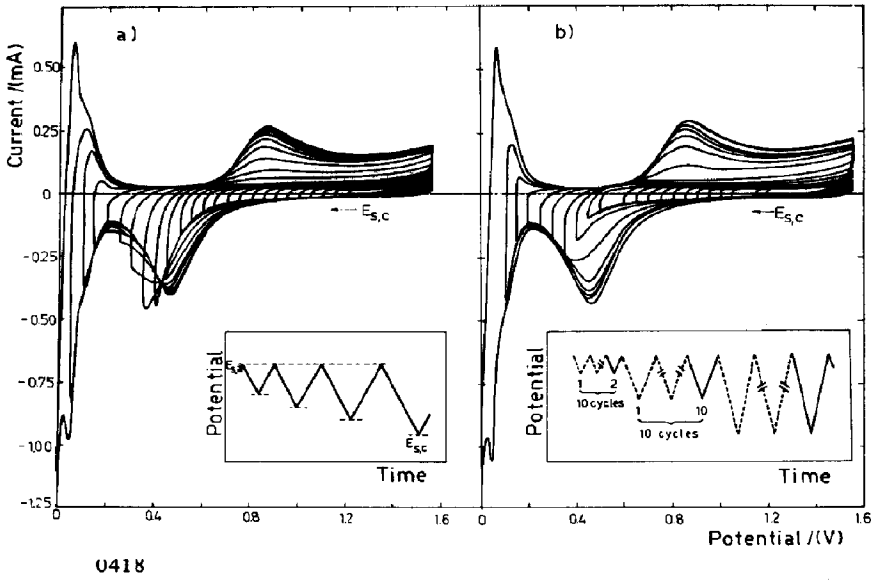

Fig. 3. Potentiodynamic E–I displays run at 0.3 V/s covering $E_{s,a} = 1.6$ V and gradually decreasing $E_{s,c}$. 12 M H_2SO_4. (a) $E_{s,c}$ is stepwise decreased from 1.2 V to 0 V during the successive TPS. (b) $E_{s,c}$ is stepwise changed as in (a) but each $E_{s,c}$ is maintained during ten RTPS. The E–I record corresponds to the 10th potential scan.

from the E–I displays with $E_{s,a}$ gradually decreasing at constant v (Fig. 5), exhibit two approximately linear regions separated by an inflexion at the potential $(E_{s,a})_i = 1.2 \pm 0.05$ V. The shape of the Q_a *vs* $E_{s,a}$ as well as the charge $(Q_a)_i$ associated to $(E_{s,a})_i$ depend notoriously on v.

Similarly the cathodic charge (Q_c) *vs* v plot at each $E_{s,a}$ (Fig. 6) also exhibits a limiting charge $(Q_c)_L$. In this case, however, no linear Q_c *vs* $E_{s,a}$ plots are obtained (Fig. 7). Furthermore, at constant $E_{s,a}$ and v, Q_c is always smaller than Q_a, except when $v \to 0$. In the 0.85 V to 1.075 V range (for $v \to 0$)Q_c hardly exceeds

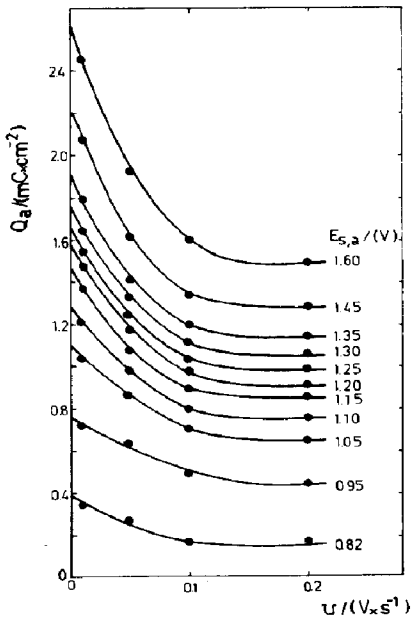

Fig. 4. Plots of the anodic charge related to the O-electrosorption *vs* the potential sweep rate at different $E_{s,a}$ values. 12 M H_2SO_4.

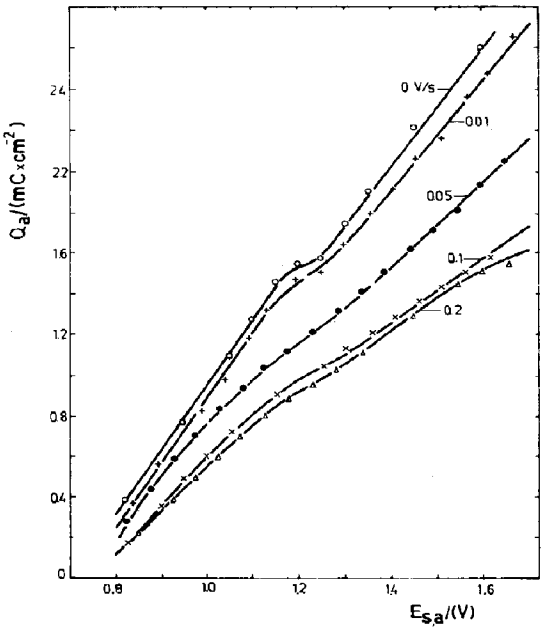

Fig. 5. Plots of the anodic charge related to the O-electrosorption *vs* $E_{s,a}$ obtained at different v. 12 M H_2SO_4.

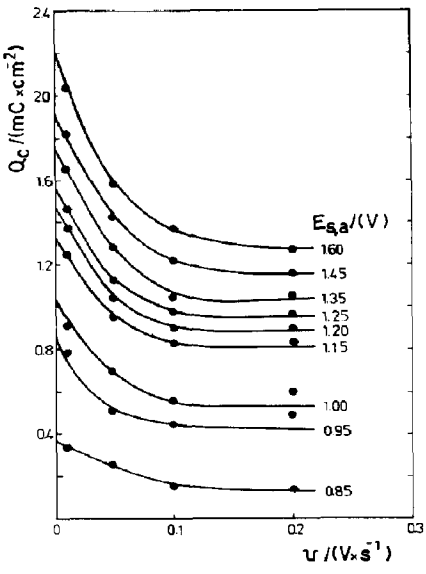

Fig. 6. Plots of the cathodic charge related to the O-electrodesorption *vs* the potential sweep rate. The different $E_{s,a}$ values are indicated in the figure. 12 M H_2SO_4.

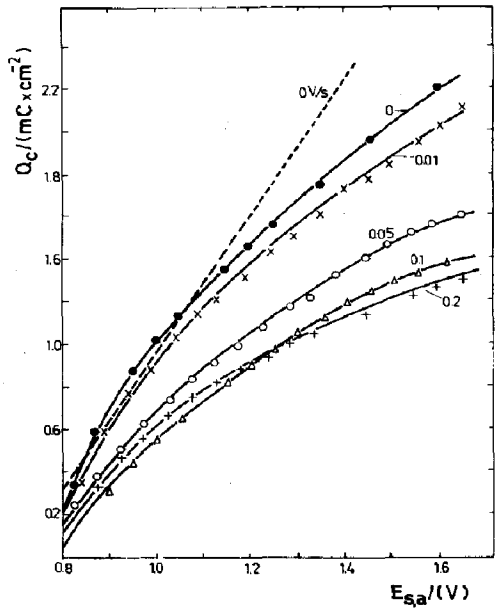

Fig. 7. Plots of the cathodic charge related to the O-electrodesorption *vs* $E_{s,a}$ obtained at different v. The dashed line corresponds to the anodic charge extrapolated at $v = 0$. 12 M H_2SO_4.

Q_a, although the small charge difference involved is within the errors of the charge evaluation and the reproducibility of the experiments.

At a constant v, the charge difference evaluated for a single triangular potential scan, $\Delta Q = Q_a - Q_c$, increases with $E_{s,a}$ particularly when $E_{s,a}$ exceeds $(E_{s,a})_i$. On the other hand, at fixed $E_{s,c}$ and $E_{s,a}$, ΔQ decreases when v increases (Fig. 8). These results indicate either that the product anodically formed involves a fraction of non-electroreducible species or that it has suffered a chemical reaction yielding different species whose electrodesorption requires a number of charges per reacting species lower than that of the electrosorption. The relative contribution of these processes should obviously depend upon the characteristics of the perturbation program applied to the electrochemical interface.

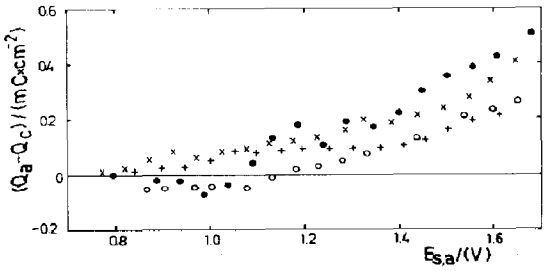

Fig. 8. Plots of the Q_a–Q_c charge difference at different v *vs* $E_{s,a}$. 12 M H_2SO_4. (●) 0.01 V/s; (x) 0.05 V/s; (+) 0.1 V/s; (○) 0.2 V/s.

Potentiodynamic aging

E–I displays were obtained by applying the potentiodynamic aging perturbation program[30, 31] covering a wide range of switching potentials ($E_{s,c}$, $E'_{s,c}$ and $E_{s,a}$) and perturbation times (τ) (Figs 9 and 10). The *E–I* response in this case depends both on the frequency of the intermediate perturbations as well as the number of potential sweeps. The results derived from the potentiodynamic aging can be divided into two groups depending on $E'_{s,c}$. Thus, when $E'_{s,c}$ is more positive than the potential of the reference O-electrodesorption current peak, during each intermediate potential perturbation cycle the anodic charge exceeds the cathodic one ($Q_a > Q_c$) and the cathodic charge (Q_c) involved in the NPS following the intermediate perturbation during the time τ results greater than the charge involved in the reference RTPS *E–I* display. Furthermore, the NPS *E–I* profile is hardly modified in the H-electrosorption potential region. On the other hand, when $E'_{s,c}$ exceeds the reference O-electrodesorption current peak potential during the successive intermediate potential cycles Q_a approaches Q_c and the charge (Q_c) determined through the NPS *E–I* profile run immediately after the intermediate RTPS perturbation hardly increases. In this case the O-electrodesorption *E–I* profile overlaps to a great extent the H-adatom electrosorption potential range. These results show that the electrochemical reactions occurring during the intermediate RTPS perturbation depend not only on v and $E_{s,a}$, but also on $E'_{s,c}$.

At a constant time τ and three different $E'_{s,c}$ located at the negative potential side of the reference O-electrodesorption current peak potential (Fig. 9b), the NPS *E–I* profile run immediately after the RTPS intermediate perturbation reveals drastic changes of

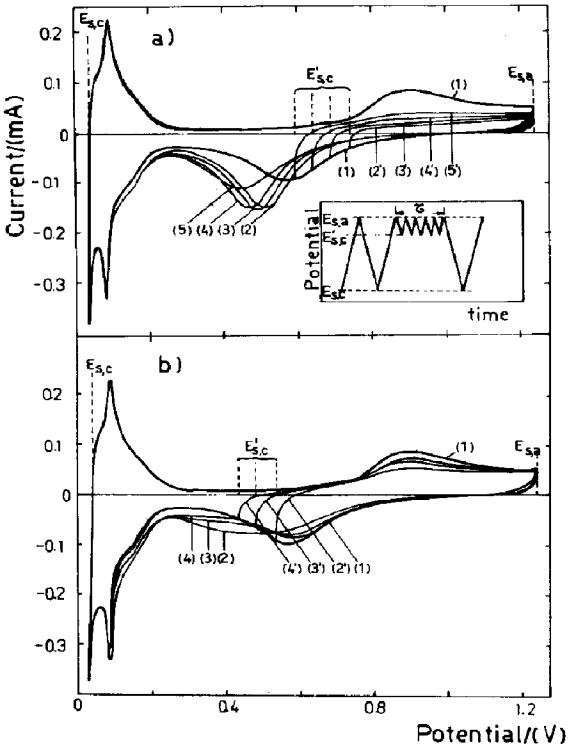

Fig. 9. E–I profiles related to the runs under potentiodynamic aging at different $E'_{s,c}$ and $\tau = 5$ min, after using the potential–time program included in the figure. The reference E–I display is denoted by (1). $v = 0.03$ V/s and $v_i = 0.03$ V/s. The last intermediate TPS is indicated by a prime number and the immediately following TPS E–I display between $E_{s,a}$ and $E_{s,c}$ is denoted by the same plain number. 12 M H_2SO_4. (a) The $E'_{s,c}$ values are more positive than the potential of the cathodic current peak in the reference E–I display. (b) The $E'_{s,c}$ values are more negative than the potential of the cathodic current peak in the reference E–I display.

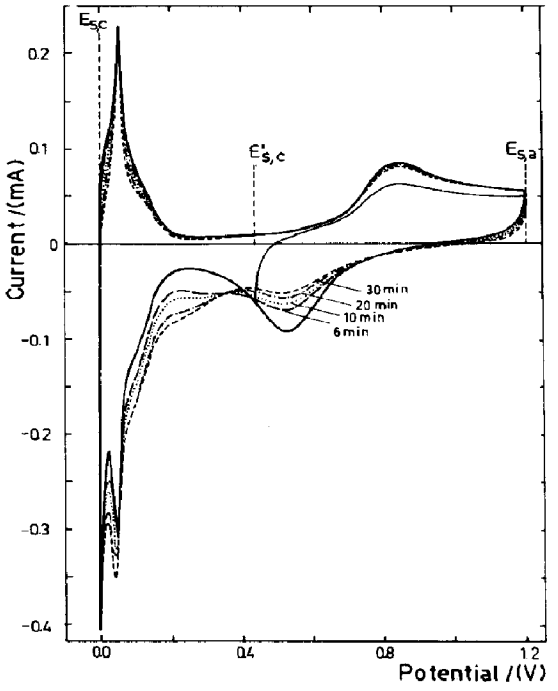

Fig. 10. E–I profiles related to the runs under potentiodynamic aging at constant $E'_{s,c}$ and different τ. $v = 0.03$ V/s and $v_i = 0.03$ V/s. 12 M H_2SO_4. See legend in Fig. 9a to complement the description of the experiments.

the O-electrodesorption E–I profile as compared to the reference one, although in any case the overall cathodic charge remains practically unaltered. The structure of the O-electrodesorption involves at least two distinguishable broad partially overlapping current peaks whose peak potential difference is of the order of 0.2 V. The resolution of the current peak multiplicity is enhanced when the charge playing part in the intermediate RTPS is greater than 60 per cent of the charge of the O-electrodesorption peak in the reference E–I display. These results correlate with those of the E–I profiles resulting from the runs where $E_{s,c}$ is stepwise changed (Figs. 3a and 3b). Otherwise, when the same type of experiments are made by fixing $E'_{s,c}$ at potentials more positive than the potential of the reference O-electrodesorption current peak (Fig. 9a), the influence of the intermediate RTPS is slightly different to that described previously seeing that no clearcut splitting of the cathodic current peak is noticed but only a single cathodic contour shifted towards the negative potential side. In addition, a slight excess of the anodic charge component is made up during each intermediate RTPS. Consequently, the overall cathodic charge recorded in the NPS after the intermediate RTPS becomes greater than that of the reference E–I display. Accordingly, during the intermediate RTPS perturbation the surface becomes covered with apparently more stable species which are not removed during the potential scan from $E_{s,a}$ down to $E'_{s,c}$. In this case, the anodic and the cathodic charges involved during the intermediate RTPS gradually decrease. This means that as the potentiodynamic aging proceeds the concentration of the O-species available for aging gradually decreases and the formation of the more reactive O-electrosorbed species is progressively hindered.

The NPS E–I displays run between $E_{s,a}$ and $E_{s,c}$ immediately after the RTPS intermediate perturbation between $E'_{s,c} = 0.44$ V and $E_{s,a} = 1.2$ V (Fig. 10) reveal a progressive shift of the O-electrodesorption charge towards the more negative potential peak as τ increases. At the same time a slight increase of the corresponding cathodic charge is noticed and the baseline related to the H-electrosorption is increased. This effect is quite likely related to the electrodesorption of a part of the potentiodynamically aged O-species at potentials ranging in the H-electrosorption potential. Moreover, under the perturbation conditions of Fig. 10 the NPS E–I profile run after the intermediate RTPS defines a net isopotential at *ca* 0.4 V. The corresponding $E'_{s,c}$ appears related to the potential of the maximum influence of the gradually changing $E_{s,c}$ on the E–I profile depicted in Fig. 3.

When $E'_{s,c}$ is more positive than the potential of the reference O-electrodesorption current peak (Fig. 11)

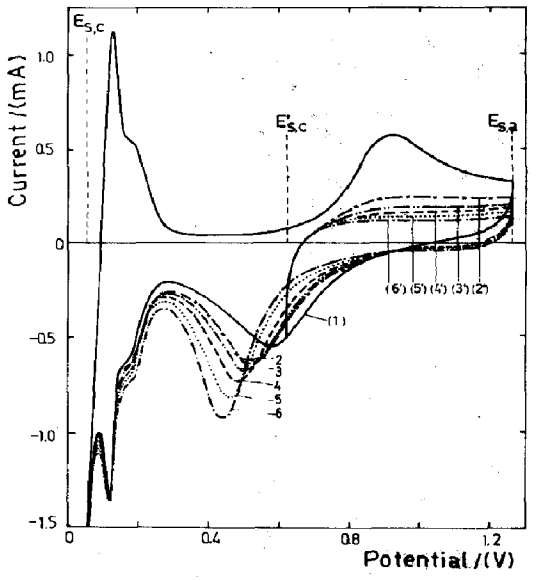

Fig. 11. Influence of the number of intermediate RTPS on the E/I display resulting after the potentiodynamic aging. 1.2 M H_2SO_4. $v = 0.3$ V/s; $v_i = 0.3$ V/s. Reference E–I profile (1) 2 cycles (2'); 3 cycles (3'); 5 cycles (4'); 10 cycles (5'); 20 cycles (6')

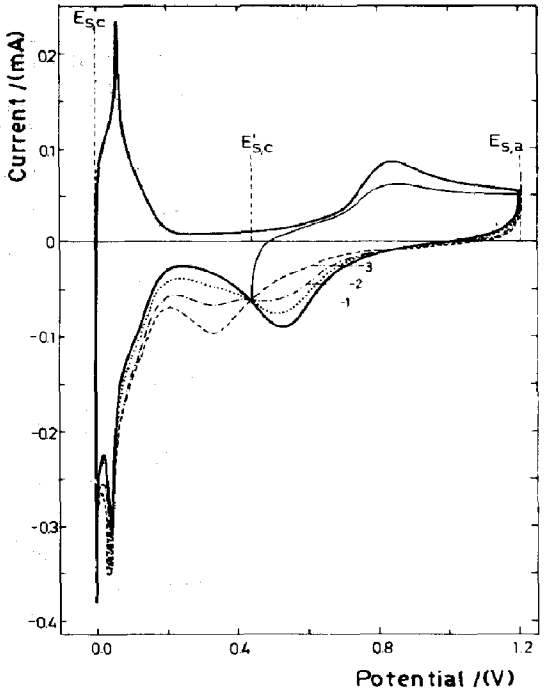

Fig. 12. Influence of v_i on the E–I display resulting after the potentiodynamic aging at constant $E'_{s,c}$ and $\tau = 2$ min. 1.2 M H_2SO_4. $v_i = 0.03$ V/s (1); $v_i = 0.30$ V/s (2) and 3.00 V/s (3).

the O-electrodesorption current peak resulting after the intermediate RTPS shifts towards more negative potentials being able to distort the E–I profile in the H-electroformation potential range. Under these circumstances, when τ increases beyond a certain time the electrodesorption E–I display of the potentiodynamically aged O-species becomes more symmetric. Simultaneously the cathodic charge exceeds the charge recorded in the reference E–I profile.

By properly adjusting either $E'_{s,c}$ or τ, the influence of the RTPS intermediate perturbation frequency is accomplished (Fig. 12). The transition from the more to the less reactive O-electrosorbed state is enhanced according as the potential sweep rate of the intermediate perturbation (v_i) increases. The greatest potentiodynamic aging effect is attained at the largest perturbation frequency (20 Hz).

These results suggest a gradual increase in stability of the O-electrosorbed species as τ and v_i increases. As the total charge Q_c remains constant at least when the potential perturbations are confined within a certain potential range, then the systematic changes in the NPS E–I display can be associated to a potentiodynamically assisted transition between two well defined O-containing surface species with the same oxidation state.

The triangularly modulated triangular potential sweep E–I *displays*

The E–I contours resulting from the application of the TMTPS (Fig. 13) exhibit during the PPS E–I display the double layer charging and discharging currents and anodic and cathodic faradaic currents corresponding to the relatively fast responses of both the H- and in the O-electrosorption processes. Under the perturbation condition of Fig. 13 during the PPS the cathodic charge is smaller than the anodic charge and the separation of the potentials of the conjugated current peaks indicate that the electrochemical reactions involved in the early stages of the O-electrosorption are not completely reversible. The degree of irreversibility of those reactions becomes more noticeable as the potential becomes more positive.

During the NPS TMTPS E–I contour the irreversibility of the processes related to the O-electrosorption/O-electrodesorption is appreciably enhanced. Thus, the O-electrodesorption current envelope becomes broad and the complementary faradaic anodic current envelope results comparatively small. This is an indication that the initial O-electrosorption product during the time the potential excursion lasts acquires a more stable configuration. Likewise, in the H-potential range, the response of the corresponding reactions is practically the same as those already described for the PPS, although the distribution of the anodic and the cathodic charges in now justly reversed.

Potentiodynamic E–I *displays after holding the potential at* $E_{s,a}$

The NPS E–I displays obtained with trapezoidal perturbation functions show the systematic increase of the cathodic charge simply by increasing the time τ the potential is held at $E_{s,a}$ (Fig. 14).

The Q_c *vs* ln τ plots (Fig. 15) furnish data about the kinetics of the growth of the O-containing species.

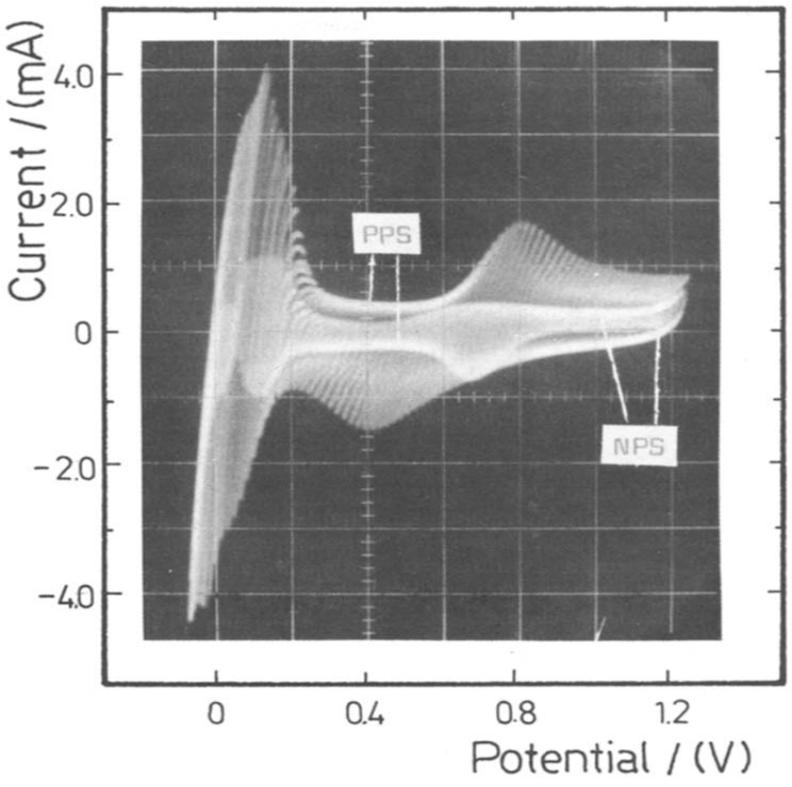

Fig. 13. *E–I* contours obtained under a triangularly modulated single triangular potential sweep. $v_{\text{basc signal}} = 1$ V/s; $v_{\text{modulting signal}} = 10$ V/s; amplitude of the modulating signal 0.1 V. 12 M H_2SO_4.

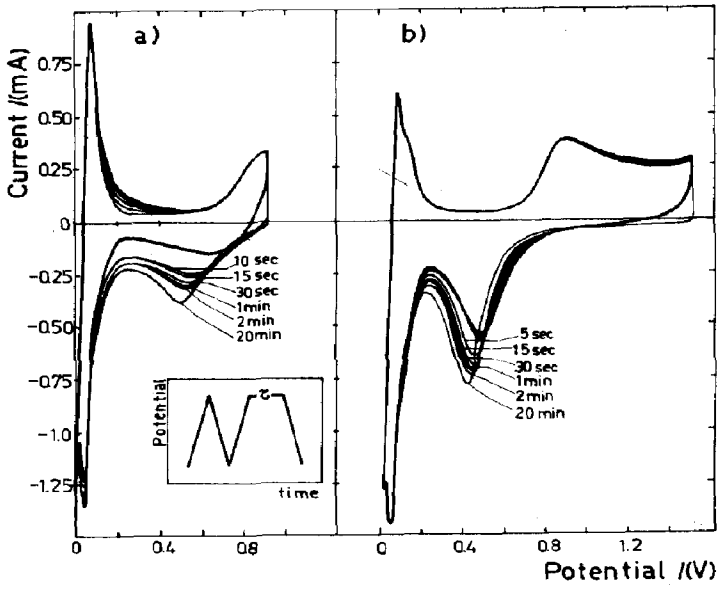

Fig. 14. Potentiodynamic *E–I* profiles run under a trapezoidal potential sweep including a potential holding at $E_{s,a}$ during different times. The perturbation program is shown in the figure. $v = 0.3$ V/s. 12 M H_2SO_4. $E_{s,a} = 0.92$ V (a) and $E_{s,a} = 1.53$ V (b).

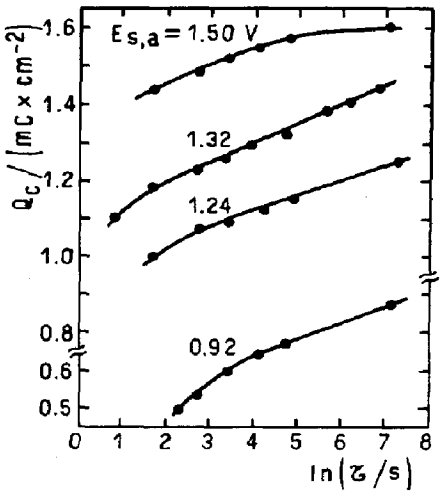

Fig. 15. Plots of the cathodic charge related to the O-electrodesorption *vs* ln τ. Data taken from experiments involving a potential holding at various $E_{s,a}$, as those shown in Fig. 14. 12 M H_2SO_4.

Thus, in the $0.92\ V \leqslant E_{s,a} \leqslant 1.5\ V$ range there is a lapse of time in which the plot fits semilogarithmic linear regions with apparently a common slope. The region of the Q_c *vs* ln τ plot preceding the linear portion ($\tau \to 0$) exhibits an increase of Q_c with ln τ which is more abrupt as $E_{s,a}$ decreases. At the largest $E_{s,a}$ in the region after the linear portion ($\tau \to \infty$), the growth of O-containing species approaches a limiting charge which is of the order of 1.60 mC/cm^2. It is about four times the charge estimated for the formation of the Rh(O) monolayer, if the roughness of the electrode approaches one although this figure seems rather unlikely. This limiting charge practically coincides with the charge derived from the Q_a *vs* $E_{s,a}$ plot (Fig. 5) at $(E_{s,a})_i$ and $v \to 0$.

DISCUSSION

Preliminary remarks

The two main overall electrochemical reactions occurring in both the diluted and the concentrate electrolyte in well defined potential ranges are related to the conjugated redox systems involving H-adatoms and the O-electrosorption–O-electrodesorption. The separation of the potential ranges of the anodic processes is better accomplished in the PPS than the separation of the potential ranges of the respective conjugated cathodic processes in the NPS. For the latter the O-electrodesorption potential range partly overlaps the potential for the initiation of the H-electroformation.

The distribution of the current peaks in the H-adatom potential range, and the initiation of the O-electrosorption depends however on the electrolyte concentration. Thus, the larger the electrolyte concentration the higher the potential of the initiation of the O-electrosorption. Furthermore, the electrolyte concentration also influences the rate of aging of the O-electrosorbed species. These effects, as in the case of the Pt/H_2SO_4 (aq) interfaces can be partly accounted for through an increasing specific anion adsorption[29]. The H-adatom electroformation and electrodesorption are relatively fast conjugated processes, particularly under slow RTPS although the corresponding peak multiplicity for the Rh/H_2SO_4 (aq) interface is apparently simpler than that already known for the Pt/H_2SO_4 (aq) interface.

The reactions in the hydrogen adatom potential range

The degree of coverage of Rh with H adatoms in 1 M H_2SO_4 has been estimated as 0.59 at $E = 0.07$ V[16]. The calculation of this figure was based on the assumption that an oxygen electrosorbed monolayer was formed on Rh at $E = 1.5$ V. Exactly the same result is obtained for the 12 M H_2SO_4 electrolyte after considering that the charge related to the O-electrosorbed monolayer corresponds to the Rh/O ratio equal to one at 1.2 – 1.3 V and $v \to 0$. It has been advanced that the charge for the H adatom monolayer on polycrystalline Rh results equal to 221 μC/cm^2[11], but in contrast, it has been reported[17] that all the specifically adsorbed anions lead to a decrease in the total adsorbed H adatom content on Rh.

The existence of at least two types of adsorption sites for H on Rh is recognized through the quantitative data obtained in 1 N H_2SO_4 on the variation of the differential heat of adsorption with the degree of H adatom coverage. This conclusion agrees with the fact that the ratio of the H adatom current peaks is influenced by the crystallographic structure of the metal. This influence is less noticeable up on increasing the temperature[24]. The H adatom coverage exhibits two different regions one approaching a Temkin adsorption isotherm at intermediate surface coverages and another a Freundlich isotherm at surface coverages lower than 0.2[5, 7, 13]. The definition of the H doublet in the potentiodynamic E–I display is enhanced by increasing the electrolyte concentration, but the proportion of the strongly bound H adatoms apparently does not decrease at high acid concentration as compared to results obtained from more diluted acids[18].

In principle, the general reaction pathways advanced for the dynamic response of the H and O electrosorbed layers on Pt apply also to the Rh/H_2SO_4 (aq) interfaces. If one admits that the H adsorption sites on Rh distribute between sites of high and low adsorption energy, the formal electrochemical reactions associated to the H adatoms can be put forward as follows:

$$(Rh)_I + H^+ + e = (Rh)_I(H) \qquad (1a)$$

$$(Rh)_{II} + H^+ + e = (Rh)_{II}(H) \qquad (1b)$$

where the subscripts I and II stands for the two types of adsorption sites. Reactions (1a) and (1b) are fast electron transfer reactions. To achieve a further understanding of these reactions since the range of potentials corresponding to the charging of the dl capacitance is narrower in the case of Rh than in the case of Pt, it is necessary to study in detail the overlapping of the H and O electrosorption and electrodesorption potential regions.

The reactions in the oxygen electrosorption and electrodesorption potential range

The potential of the O-electrosorption reactions can, in principle, be related to the standard equilibrium potentials (E°) of the following electrochemical reactions involving different rhodium oxides[32]:

$$Rh + H_2O = Rh_2O + 2H^+ + 2e \quad E^\circ = +0.796\ V \quad (2a)$$
$$Rh_2O + 2H^+ = 2Rh^{3+} + H_2O + 4e \quad E^\circ = +0.801\ V \quad (2b)$$
$$Rh_2O + 2H_2O = Rh_2O_3 + 4H^+ + 4e \quad E^\circ = +0.877\ V \quad (2c)$$

and

$$Rh_2O + H_2O = 2RhO + 2H^+ + 2e \quad E^\circ = +0.886\ V \quad (2d)$$

Among these reactions, the chemical equilibrium related to the disproportion of the Rh(II) species into Rh(I) and Rh(III) species according to

$$4RhO = Rh_2O + Rh_2O_3 \quad (3)$$

should also be considered. Reaction (3) is an exothermic reaction, $\mu = -0.50$ Kcal/mol Rh_2O. Hence, from the thermodynamic viewpoint, three stoichiometries can be associated to Rh–O compounds namely RhO, Rh_2O and Rh_2O_3. These stoichiometries which characterize bulk compounds, can not however straightforwardly be extended to the surface species generated through the electrosorption processes.

Some idea about the type of O-surface species electrochemically formed on Rh can be obtained from the Q_s *vs* $E_{s,a}$ and Q_a *vs* v plots (Figs. 4 and 5). The potential $(E_{s,a})_i = 1.2 \pm 0.05$ V which defines the transition between two approximately linear portions in the Q_a *vs* $E_{s,a}$ plot seems adequate for the purpose. This can be associated to the potential at which the monolayer of an O-containing species is already formed. For this monolayer the Rh_2O_3 stoichiometry seems rather unlikely seeing that it would correspond to an oxide film completely separated from the metal lattice. At the surface level the oxygen monolayer electrosorption saturation at $(E_{s,a})_i$ would be probably better conceived by the limiting Rh–O stoichiometric ratio equal to one as in Pt[16, 19]. However, the relatively poor stability of RhO suggests that the surface species already at $E_{s,a} < (E_{s,a})_i$ according to (3) transforms into a mixture of Rh_2O and Rh_2O_3 surface species. The relative surface transient concentrations of these species should obviously depend upon the perturbation conditions applied to the interface and on the rate constant of (3). Accordingly the charge increases operating at $E_{s,a} > (E_{s,a})_i$ should imply the formation of oxygen containing surface species where the Rh–O stoichiometric ratio becomes lower than one.

The Q_a *vs* v plot at different $E_{s,a}$ (Fig. 4) exhibits firstly an initial decay and then a limiting charge $(Q_a)_L$ which is attained practically at the same v in the $0.8\ V \leqslant E_{s,a} \leqslant 1.6$ V range (Fig. 16). Both the initial decay slope and the value of $(Q_a)_L$ increase as $E_{s,a}$ increases. The continuity of the Q_a *vs* $E_{s,a}$ plots (Fig. 5) at different v suggests that within the 0.8 V to 1.6 V range, the stoichiometry of the overall reaction remains in principle, the same so that the dependence of either Q_a on $E_{s,a}$ at constant v or the dependence of Q_a on v at a constant $E_{s,a}$, should be associated to another major type of influence on the complex electrochemical reaction such as the specific adsorption of anions at the Rh surface. For the electrolyte used the HSO_4^- anion is the predominant adsorbable species on Rh at positive potential[21]. Its adsorption fits a Roginskii–Zeldovich kinetic equation with a Temkin isotherm. The interference of anion adsorption during the potentiodynamic O-electrosorption and electrodesorption is concluded from the fact that the time required to attain the charge $(Q_a)_L$ calculated as $(E_{s,a} - E_{s,c})/v$, which is comprised between about 10 s/cycle for any perturbation conditions between the 0.8 V to 1.6 V range, is within the order of magnitude of the time required to attain the maximum ionic adsorption of the HSO_4^- ion on Rh[21]. Consequently, it is reasonable to admit that no HSO_4^- ion equilibrium adsorption is established for the 12 M H_2SO_4 electrolyte when potentiodynamic sweeps last no less than 5–10 s. Therefore, at the fastest potential sweeps the initial equilibrium concentration of adsorbed anions would remain practically unaltered and the influence of adsorbed ionic species on the O-electrosorption would be maximum. For the Rh–12 M H_2SO_4 interface this is accomplished when the v value related to $(Q_a)_L$ is exceeded. The reverse limiting situation should be achieved at $v \to 0$, that is when the conditions of a potentiostatic step function are approached. In this case, the adsorbed anion can be removed from the surface simultaneously with the O-electrosorption process so that at each particular potential the maximum number of surface sites can be provided for the O-species. The maximum number of O-electrosorbed species is then related to the charge $(Q_a)^\circ$.

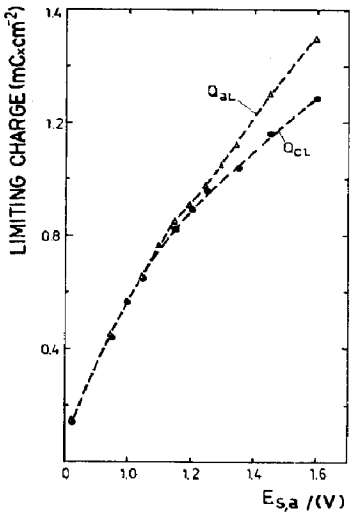

Fig. 16. Plots of the limiting anodic and cathodic charges *vs* $E_{s,a}$. 12 M H_2SO_4.

Further aspects of the complex anodic electrochemical reaction can be derived from the correlation between the Q_a *vs* v plot with both the increase of the $(Q_a - Q_c)$ charge difference with $E_{s,a}$ (Fig. 8) and the decrease of the charge difference $(Q_a)^\circ_{1.6} - Q_s$ with $E_{s,a}$ where $(Q_a)^\circ_{1.6}$ is the anodic charge read at 1.6 V, (Fig. 17) and Q_s corresponds to the charge difference $(Q_a)^\circ - (Q_a)_L$. These rather complex charge dependences can be explained through the occurrence of other less important processes in addition to the O-electrosorption, including the partial electrodissolution of Rh, the possible direct electrooxidation of Rh to

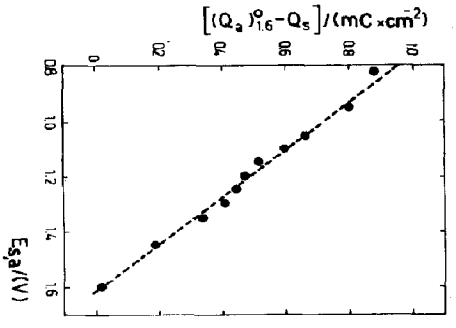

Fig. 17. Plot of the charge difference $[(Q_a)^{\circ}_{1.6} - Q_s]$ *vs* $E_{s,a}$. The definition of symbols is given in the text.

Rh(IV), the partial chemical dissolution of the electrosorbed species and the redox chemical reactions among the electrosorbed species. Furthermore, the $(Q_a - Q_c)$ charge difference may imply that the average number of charges per reacting species in the anodic process is larger than in the cathodic one.

The maximum contribution of the chemical dissolution at the Rh/12 M H_2SO_4 when $E_{s,a}$ exceeds $(E_{s,a})_i$ as estimated exclusively from the charge difference $Q_a - Q_c$, is 0.31 $\mu C/cm^2$ (0.11 $\mu g/cm^2$) of Rh. The order of magnitude of this figure coincides with that previously reported for the Rh/1 M H_2SO_4[17]. It confirms, therefore, that at different H_2SO_4 concentrations the chemical dissolution of the oxygen containing films on Rh is enhanced when compared to Pt[17]. The chemical dissolution, however, contributes to a larger extent both when $E_{s,a}$ increases and when v decreases. Thus, when $E_{s,a}$ exceeds 1.2 V, the dissolution can be explained through reactions already known from the chemistry of Rh in aqueous solutions[35–37]. Accordingly the overall reaction

$$6\,RhO = 2\,Rh_2O + Rh_2O_3 + \tfrac{1}{2}\,O_2 \qquad (4)$$

can be extended to the electrochemical interface. Rh_2O_3 is the stable species of highest valency yielded by the disproportionation reaction which in principle, can separate from surface. The formation of Rh_2O_3 according to (4) means that additional O-electrosorption is feasible at the new available Rh_2O sites. Reaction (4) may involve the following sequence of reactions[35–37]:

$$3\,RhO = Rh_2O + RhO_2 \qquad (4a)$$

$$2\,RhO_2 = Rh_2O_3 + \tfrac{1}{2}\,O_2 \qquad (4b)$$

If reaction (4) proceeds to some extent it means that while the potentiodynamic anodic reaction produces RhO, the cathodic reaction involves the electroreduction of Rh_2O and Rh_2O_3, then the upper limiting $(Q_a - Q_c)$ value should be 17 per cent the Q_a value. In this way, the $(Q_a - Q_c)$ charge difference and its dependence both of v and $E_{s,a}$ can be qualitatively accounted for. However, since the $(Q_a - Q_c)$ charge difference is positive at any v ($v \neq 0$), and $E_{s,a} > 1$, 2 and it only increases with $E_{s,a}$ at a constant v, the possible chemical formation of O-electrosorbed species which are only partially electroreduced during the NPS should also be considered. This is closely related to the overlapping of the O-electrodesorption and the H-electrosorption potential ranges, which is particularly remarkable for those electrodes which were aged at high positive potentials. This adds to the possibility of other chemical reactions between the different surface species within the potential range when their coexistence becomes feasible. In this sense, the most likely reaction is:

$$Rh(OH) + (H)Rh = H_2O + 2\,Rh \qquad (5)$$

which corresponds to a chemical reduction of the O-electrosorbed species remaining on the surface by traces of H adatoms.

The relatively large number of both the species produced by the electrochemical reactions under potentiodynamic sweeps and the possible chemical processes interfering with the former ones indicate that the conclusions derived from the charge balance in the present circumstances should be handled with care. Despite the occurrence of these processes the kinetics of the main electrochemical reactions can be discussed as has generally been the case with other noble metal electrodes, in which, to a greater or lesser extent, the preceding discussion also applies.

Aging processes related to the O-*electrosorption and* O-*electrodesorption*

The potential of the initiation of the O-electrosorption is partly influenced by the specific adsorption of anions and partly governed by the bulk properties of the metal[18]. The *E–I* characteristics of the O-electrodesorption process are strongly dependent upon the perturbation conditions applied to the interface as it was the case for Pt in similar electrolytes[27, 31, 33]. The O-electrodesorption potential which is shifted towards more negative potential furnishes evidence that part of the O-electrosorbed species becomes more tightly bound to the metal, the longer it remains on the electrode surface and the more positive the potential at which it is electrosorbed[15]. This response is associated to the aging processes occurring during the O-electrosorption as they can be demonstrated either under open circuit aging or under potentiodynamic aging[27, 33].

Through the different *E–I* profiles it is clear that the O-electrodesorption comprises two main cathodic reactions and possibly a third one. The latter can be envisaged through the composite TMTPS *E–I* display in the 0.76 V to 1.24 V range, with Type I electrodes (Fig. 13). Thus, at the highest HSO_4^- ion concentration the dissolution of Rh(IV) may be favoured, so that the possible electrodissolution of Rh to RhO^{2+} should also be considered:

$$H_2O + Rh = RhO^{2+} + 2H^+ + 4e \qquad (6)$$

Under standard conditions (6) is thermodynamically favoured when E is larger than 1.08 V[32]. There is some evidence not shown in the present work that a cathodic current peak which is observed at *ca* 1.7 V could, in principle be related to the electroreduction of the RhO^{2+} species, although this is not proven.

The O-electrodesorption *E–I* profile resulting immediately after the potentiodynamic aging at different v, between $E_{s,a}$ and $E'_{s,c}$, shows the shift of the cathodic current peak potential at a constant Q_c from its initial location at *ca* 0.62 V to *ca* 0.42 V. This potential shift is assigned to the transition from the less to the more

stable O-electrosorbed species. The latter is completely electroreduced only when the H-adatoms potential region is reached.

The O-electrosorption can be interpreted through reactions formally similar to those already advanced for the Pt–H_2SO_4(aq) interfaces. Then, the anodic reaction sequence when the potential sweep goes from $E_{s,c}$ towards $E_{s,a}$ is:

$$Rh + H_2O = Rh(OH) + H^+ + e \quad (7)$$
$$Rh(OH) = Rh(O)^* + H^+ + e \quad (8)$$
$$Rh(O)^* = Rh(O) \quad (9)$$

where the asterisk denotes the transient less stable species. Accordingly, the complementary electrodesorption reaction during the reverse potential scan can be put forward:

$$Rh(O) + H^+ + e = Rh(OH) \quad (10a)$$
$$Rh(O)^* + H^+ + e = Rh(OH) \quad (10b)$$
$$Rh(OH) + e + H^+ = Rh + H_2O \quad (11)$$

The reaction formalism depicted by (7)–(11) is based upon a monolayer formation where the Rh–O atomic ratio is equal to one. The relative contributions of each electroreduction step from (10a) to (10b) depend on the aging extent of the O-electrosorbed layer.

The (OH) electrosorption processes (steps (7) and (11)) involve a fast electron transfer in both directions as it is clearly evidenced through the TMTPS experiments[34]. Step (8), where the Rh(I) and Rh(II) surface intermediates are involved, can be related with the reactions (2a) to (2d). Accordingly, the product of step (7) as the initial stage of the overall reaction (2a), undergoes the electrochemical reaction (8) or it reacts as follows:

$$2Rh(OH) = Rh_2O + H_2O \quad (12)$$

Furthermore, as the RhO species is also formed, the participation of the equilibrium (3) becomes feasible. The difference between the TMTPS *E–I* contours in the positive and in the negative directions (Fig. 13) can be interpreted through the contribution of different states of the O-species on Rh. Thus, in the PPS, Q_a becomes hardly greater than Q_c as part of the Rh(OH) species is transformed into the Rh(O), Rh_2O and Rh_2O_3 species. Hence, the immediately following NPS *E–I* contour should depend on the relative surface concentration ratio attained for the three species. The major aging effect which is formally presented through step (9) should, however, be attributed to the formation of those species approaching the Rh_2O and the Rh_2O_3-type structure. The half-life time of the Rh(O)* species as estimated from the TMTPS is of the order of 0.5–1.0 ms, so the following restructuring reactions yielding the Rh oxides are relatively slow processes. This is coherent with the fact that the charge playing part in the potentiodynamic aging is sensitive to $E_{s,a}$.

The preceding interpretation applies to the results described earlier with the potentiodynamic aging perturbation technique. Thus, when the intermediate RTPS perturbation is confined to a relatively high positive potential range but the potential difference $(E_{s,a} - E'_{s,c})$ approaches zero, it is likely that the pertaining anodic and cathodic processes comprise different numbers of charges per reacting species. Then, apart from the anodic reactions (7)–(9) reaction (20) may be also included if (12) has occurred. Therefore, when the charge removed during the intermediate RTPS perturbation is less than one half of the monolayer charge, the accumulation of species of the Rh_2O_3-type structure is promoted. This implies the partial restructuring of the O-containing layer with simultaneous shift of the O-electrodesorption current peak towards the negative potential side and the increase of the O-electroreduction charge after the intermediate RTPS perturbation. Contrarily, when the charge playing part in the intermediate RTPS perturbation implies only the removal of a fraction of the surface species which is greater than one half of the monolayer charge, then a larger surface restructuring contribution should be induced. Consequently, the formation of Rh(O) species of greater stability and the likely penetration of the O species into the metal lattice beyond the layer defining the metal plane should be favoured.

The results obtained with intermediate potentiodynamic perturbations where $E'_{s,c}$ is more negative than the O-electrosorption current peak potential in the reference *E–I* profile, can also be explained through a greater restructuring promoted by lateral repulsion interactions of the O-sorbed species which can also assist the splitting of the O-electrodesorption *E–I* profile, as it has been suggested for thermal sorptive processes[38].

On the basis of the preceding discussion the O-electrosorption processes on Rh in the H_2SO_4 electrolytes can be summarize in terms of a complex film electroformation mechanism involving at least two alternative reaction pathways both of which comprise electrochemical and chemical steps. If any chemical dissolution contribution and influence of the anion specific adsorption are neglected, the reaction mechanism can be put forward as follows:

$$\text{(I)}\quad Rh + H_2O \underset{e}{\overset{-H^+}{\rightleftharpoons}} Rh(O) \underset{e}{\overset{*-H^+}{\rightleftharpoons}} Rh(O) \underset{e}{\rightleftharpoons} \rightleftharpoons Rh(III)\ \text{surf. species.}$$

$$\text{(II)}\quad Rh + H_2O \underset{e}{\overset{-H^+}{\rightleftharpoons}} Rh(O) \underset{e}{\overset{*-H^+}{\rightleftharpoons}} Rh(O) \rightleftharpoons \rightleftharpoons [Rh(I) + Rh(III)]\ \text{surf. species.}$$

Reaction pathway I involves three successive electron transfer steps while reaction pathway II comprises a chemical stage finally producing different O-species which gradually block the electrode surface. The latter predominates as $v \to 0$, and involves the formation of the most stable mixture of surface species and it implies the largest $(Q_a - Q_c)$ charge difference. Under the limiting conditions of reaction pathway II, the surface oxide layer increases linearly with the anodic potential (Fig. 5) as the film thickness increases. The potential independent pseudocapacitance associated to the film growth suggests that the latter occurs under a constant potential gradient.

Reaction pathway I represents the limiting situation as $v \to \infty$. In this case, the consecutive electron transfer reactions proceed without any appreciable interference of the aging process but the film growth is apparently similar to that involved under reaction pathway II.

The interpretation of the electrochemical behaviour of the Rh/H_2SO_4 interfaces throws further light onto

two relevant aspects of the oxygen electrosorption which applies to other noble metal–H_2SO_4 interfaces. Firstly, the type of place exchange mechanism associated to the restructuring of the film predominantly occurs through the O–M type species instead of the OH–M type species. The M(OH) species participate principally in the initial stages of the process through fast single electron transfer reactions. Secondly, the aging processes, which are still not well defined in structural terms, should imply among other physical changes in the film, the occurrence of disproportionation reactions such as that represented by reaction (3). As in the case of Ru[39–43] the aging process is also probably more complex involving Rh–O–Rh bridges dependent on the valence state of Rh and on protonation.

Acknowledgement—INIFTA is sponsored by the Consejo Nacional de Investigaciones Cientificas y Técnicas, the Universidad Nacional de La Plata and the Comisión de Investigaciones Cientificas (Provincia de Buenos Aires). This work was partially supported by the Regional Program for the Scientific and Technological Development of the Organization of the American States.

REFERENCES

1. M. W. Breiter, C. A. Knorr and M. Völkl, *Z. Elektrochem.* **59,** 681 (1955).
2. G. Bélanger and A. K. Vijh, in *Oxides and Oxide Films,* Vol. 5 (Edited by A. K. Vijh) p. 1. M. Dekker, New York (1977).
3. F. G. Will and C. A. Knorr, *Z. Elektrochem.* **64,** 258 (1960).
4. Yu. M. Tyurin, *Dokl. Akad. Nauk SSSR* **126,** 827 (1959).
5. W. Böld and M. W. Breiter, *Z. Elektrochem.* **64,** 897 (1960).
6. W. Böld and M. W. Breiter, *Electrochim. Acta* **5,** 145 (1961); *ibid* **5,** 169 (1961).
7. M. W. Breiter, *Ann. N. Y. Acad. Sci.* **101,** 709 (1963).
8. J. P. Hoare, *J. electrochem. Soc.* **111,** 232 (1964).
9. J. Llopis and M. Vázquez, *Electrochim. Acta* **9,** 1655 (1964).
10. E. I. Khruscheva, N. A. Shumilova and M. R. Tarasevich, *Elektrokhimiya* **2,** 277 (1966).
11. M. R. Tarasevich, K. A. Radyushkina and R. Kh. Burshtein, *Elektrokhimiya* **3,** 221 (1967).
12. T. Biegler, *J. electrochem. Soc.* **114,** 1261 (1967).
13. R. V. Marvet and O. A. Petrii, *Elektrokhimiya* **3,** 1445 (1967).
14. T. Biegler, *J. electrochem. Soc.* **116,** 1131 (1969).
15. R. Kh. Burshtein, M. R. Tarasevich and K. A. Radyushkina, *Elektrokhimiya* **6,** 1611 (1970).
16. D. A. J. Rand and R. Woods, *J. electroanal. Chem.* **31,** 29 (1971).
17. D. A. J. Rand and R. Woods, *J. electroanal. Chem.* **35,** 209 (1972).
18. A. Capon and R. Parsons, *J. electroanal. Chem.* **39,** 275 (1972).
19. B. V. Tilak, B. E. Conway and H. Angerstein-Kozlowska, *J. Electroanal. Chem.* **48,** 1 (1973).
20. C. M. Ferro, A. J. Calandra and A. J. Arvia, *J. electroanal. Chem.* **55,** 291 (1974); *ibid* **59,** 239 (1975).
21. M. S. Chemeris, A. G. Stromberg and Yu. B. Vasiliev, *Elektrokhimiya* **11,** 560 (1975).
22. B. E. Conway and H. Angerstein-Kozlowska, *Electrocatalysis on Non-Metallic Surfaces,* Proceedings of Workshop help at NBS, p. 107 (1976).
23. R. Woods in *Electroanalytical Chemistry* (Edited by A. J. Bard), Vol. 9, p. 1. Arnold Press, London (1977).
24. A. M. Meretskii, I. V. Kudryashov and Yu. B. Vasiliev, *Elektrokhimi* **13,** 147 (1977).
25. H. Angerstein-Kozlowska, B. E. Conway, B. Barnett and J. Mozota, *J. electroanal. Chem.* **100,** 417 (1979).
26. N. R. Tacconi, A. J. Calandra and A. J. Arvia, *J. electroanal. Chem.* **57,** 325 (1974).
27. N. R. de Tacconi, A. J. Calandra and A. J. Arvia, *J. electroanal. Chem.* **51,** 25 (1974).
28. B. E. Conway, N. Angerstein-Kozlowska and E. Criddle, *Analyt. Chem.* **45,** 1331 (1973).
29. R. O. Lezna, N. R. de Tacconi and A. J. Arvia, *J. electrochem. Soc.* **126,** 1240 (1979).
30. N. R. de Tacconi, J. O. Zerbino, M. E. Folquer and A. J. Arvia, *J. electroanal. Chem.* **85,** 213 (1977).
31. M. E. Folquer, J. O. Zerbino, N. R. de Tacconi and A. J. Arvia, *J. electrochem. Soc.* **126,** 592 (1979).
32. M. Pourbaix, *Atlas of Electrochemical Equilibria in Aqueous Solutions,* Pergamon Press (1966).
33. J. O. Zerbino, N. R. de Tacconi, A. J. Calandra and A. J. Arvia, *J. electrochem. Soc.* **124,** 475 (1977).
34. N. R. de Tacconi, J. O. Zerbino and A. J. Arvia, *J. electroanal. Chem.* **79,** 287 (1977).
35. W. M. Latimer, *Oxidation potentials* 2nd edn, Prentice Hall Inc. (1952).
36. S. E. Livingstone, *Comprehensive Inorganic Chemistry,* Vol. 3, (Edited by J. C. Bailar, H. J. Emeléus, R. Yholm and A. Trotman-Dickenson) Pergamon Press, (1973).
37. T. J. Walsh and E. A. Hausman, *Treatise on Analytical Chemistry* part II, Vol. 8 (Edited by I. M. Kolthoff and P. J. Elving), Interscience (1963).
38. D. L. Adams, *Surface Sci.* **42,** 12 (1974).
39. S. Hadzi-Jordanov, H. Angerstein-Kozlowska, M. Vukovic and B. E. Conway, *J. electrochem. Soc.* **125,** 1471 (1978).
40. W. P. Griffin, *The Chemistry of the Rarer Platinum Metals,* Chap. 4, Interscience, London (1967).
41. J. Dunwitz and L. E. Orgel, *J. Chem. Soc.* 2594 (1953).
42. L. D. Burke, J. K. Mucahy and S. Venkatesan, *J. electroanal. Chem.* **73,** 207 (1976); *ibid* **81,** 339 (1977).
43. J. McBreen, in *Power Sources,* Vol. 5 (Edited by D. H. Collins) p. 525. Academic Press, London (1975).